Nanoscale

Accepted Manuscript

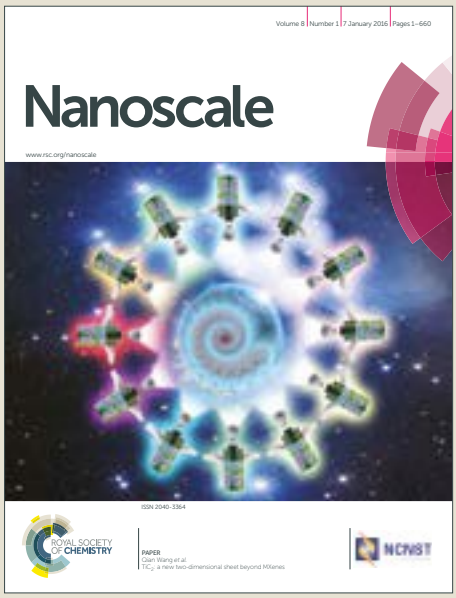

ROYAL SOCIETY OF CHEMISTRY

rsc.li/nanoscale

View Article Online
DOI: 10.1039/C7NR05013E

Heterogeneous and self-organizing mineralization of bone matrix promoted by hydroxyapatite nanoparticles

G. Campi[a°], F. Cristofaro[b,c°], G. Pani[d], M. Fratini[e,f], B. Pascucci[a], P.A. Corsetto[d], B. Weinhausen[g], A. Cedola[e], A.M. Rizzo*[d], L. Visai*[b,c], G. Rea*[a]

[a] Institute of Crystallography - CNR, via Salaria Km 29.300, 00015, Monterotondo Roma, Italy

[b] Molecular Medicine Department (DMM), Center for Health Technologies (CHT), UdR INSTM, University of Pavia, Viale Taramelli 3/B – 27100 Pavia – ITALY

[c] Department of Occupational Medicine, Toxicology and Environmental Risks, Istituti Clinici Scientifici Maugeri S.p.A, IRCCS, Via S. Boezio, 28 - 27100 Pavia – ITALY

[d] Department of Pharmacological and Biomolecular Sciences, Università degli Studi di Milano, via D. Trentacoste 2, 20134 Milano, Italy.

[e] Institute of Nanotechnology-CNR c/o Physics Department at 'Sapienza' University, Piazzale Aldo Moro 2, 00185 Rome, Italy

[f] Fondazione Santa Lucia I.R.C.C.S., Via Ardeatina 306, 00179 Roma, Italy

[g] European Synchrotron Radiation Facility, B. P. 220, F-38043 Grenoble Cedex, France

° Both authors contributed equally to this article

***Corresponding authors:**

giuseppina.rea@ic.cnr.it, angelamaria.rizzo@unimi.it, livia.visai@unipv.it

View Article Online
DOI: 10.1039/C7NR05013E

Abstract

The mineralization process is crucial to the load-bearing characteristics of the bone extracellular matrix. In this work, we have studied the spatiotemporal dynamics of mineral deposition by human bone marrow mesenchymal stem cells differentiating toward osteoblasts promoted by the presence of exogenous hydroxyapatite nanoparticles. At molecular level, the added nanoparticles positively modulated the expression of bone-specific markers and enhanced calcified matrix deposition during osteogenic differentiation. The nucleation, growth and spatial arrangement of newly deposited hydroxyapatite nanocrystals have been evaluated using Scanning Micro X-Ray Diffraction and Scanning Micro X-Ray Fluorescence. As leading results, we have found the emergence of a complex scenario where the spatial organization and temporal evolution of the process exhibit a heterogeneous and self-organizing dynamics. At the same time the possibility to control the differentiation kinetic through the addition of synthetic nanoparticles, paves the way to empower the generation of more structured bone scaffolds in tissue engineering and to design new drugs in regenerative medicine.

Keywords: Biomineralization, Bone Marrow Stem Cells, Scanning X-ray micro-diffraction, Spatial statistics, Nanoparticles, Hydroxyapatite.

View Article Online
DOI: 10.1039/C7NR05013E

1. Introduction

Bone is a complex hierarchical structure where the interplay of organic and inorganic mineral phases at different length scale affects its functional and physical-chemical properties. The biological process of bone matrix mineralization involves the deposition of an inorganic mineral phase through a series of different and complex events carried and regulated by osteoblasts. In particular, this process is strictly related to the osteoblast differentiation from mesenchymal stem cells following timely programmed steps requiring the expression of specific genes, which in turn are under the control of pro-osteogenic pathways. *Runt-related transcriptional factor 2* (Runx2) is reported as the master gene in early stages of osteoblast differentiation, during which osteoblast progenitors acquire bone-specific alkaline phospatase (ALP), an early marker of osteoblast differentiation.[1] At this differentiation stage, these cells, that are pre-osteoblasts, undergo morphological changes, becoming large and cuboidal, highly positive for ALP activity and very active in the synthesis of the extracellular matrix (ECM), mainly consisting of type-I collagen (Col-I).[2] The late stage of osteoblast differentiation is characterized by increased levels of Col-I, and by the production of non-collagenous proteins such as bone sialo protein (BOSP), osteopontin (OPN), osteonectin (ONT), osteocalcin (OCN) and decorin (DCN). OPN is important in stabilizing the matrix, while OCN is a highly carboxylated protein, almost exclusively expressed in bone and upregulated in the late differentiation stage.[3,4] This stage coincides with the onset of mineralization where hydroxyapatite nanocrystals nucleate and grow in an organic collagenous matrix forming a heterogeneous tissue where the structural properties can change point by point at different length scale.[5, 6] This makes it quite difficult to model structural features with conventional experimental approaches, requiring high spatial resolution probes. Scanning Synchrotron radiation techniques, such as Scanning micro X-ray Diffraction (SμXRD) constitute a very effective methodology in the multiscale structural study of heterogeneous matter in different research fields ranging from material science, nanotechnology up to biomedicine.[7-10]

In this work we have first characterized the deposited ECM in cell monolayers samples studying gene expression alongside protein composition at two different significant differentiation times (e.g. 8 and 28 days) in presence and absence of exogenously supplied hydroxyapatite nanoparticles (nHap). Then we have studied the spatiotemporal dynamic of the hBM-MSC differentiation by measuring the forming hydroxyapatite nanocrystal amount in the same samples by the simultaneous application of SμXRD

View Article Online
DOI: 10.1039/C7NR05013E

and Scanning micro X-ray Fluorescence (SμXRF).[11] This will give deeper information on temporal and spatial organization of cell signaling pathways and how this organization can be controlled in a nano-technological approach with the use of nHap. The results are expected to offer a worthy contribution both in applicative science by generating more structured and organized scaffolds for bone tissue engineering, and in basic science providing more sophisticated and complex models for stem cell differentiation, against the simplifying homogeneity assumption.

2. Materials and Methods

2.1. Primary human bone marrow mesenchymal stem cell culture

The Institutional Review Board of the University of Pavia (2011) approved the design of this study. Bone Marrow (BM) aspirates were harvested from healthy pediatric hematopoietic stem cell donors after obtaining written informed consent. Thirty milliliters of BM from each donor was assigned to Bone Marrow Mesenchymal Stem Cell (hBM-MSC) generation; heparin was added as an anticoagulant. Mononuclear cells were isolated from BM aspirates (30 mL) by Ficoll density gradient centrifugation (density, 1.077 g/mL; Lymphoprep, Nycomed Pharma, Oslo, Norway) and plated in non-coated 75- to 175-cm^2 polystyrene culture flasks (Corning Costar, Celbio, Milan, Italy) at a density of 16 x 10^4 cells/cm^2. Cells were cultured in proliferative medium composed by Mesencult medium (Stem Cell Technologies, Vancouver, Canada) supplemented with 2mM L-glutamine, 50 μg/mL gentamycin, and 10% fetal calf serum. Cultures were maintained at 37°C in a humidified atmosphere containing 5% CO_2. After 48 h, non-adherent cells were discarded and culture medium was replaced twice a week. After reaching 80% confluence as a minimum, the cells were harvested and re-plated for expansion at a density of 4000 cells/cm^2 until the fifth passage. The colony-forming unit fibroblast assay (CFU-F) was performed as described previously.[12] CFU-F formation was examined after 12 days of incubation in a humidified atmosphere (37°C, 5% CO_2); the clonogenic efficiency was calculated as the number of colonies per 10^6 BM mononuclear cells seeded. According to the International Society for Cellular Therapy on the nomenclature of mesenchymal progenitors, the cells cultured for this study were defined as multipotent stromal cells. To phenotypically characterize BM-MSCs and to define their purity, FACS analysis was performed as previously described. After reaching 80% confluence at a minimum, the cells were harvested and re-plated for

View Article Online
DOI: 10.1039/C7NR05013E

expansion at a density of 2.5 x 10^4 cells/cm^2. The cells were cultured at 37°C, 5% CO_2, and three fifths of the medium was renewed every 3 days.

2.2. Nanoparticles preparation and characterization

Hydroxyapatite nanopowder was synthesized with sol-gel technique as previously described[13]. To obtain a stable nHap suspension, 5 mg of sterile synthesized pure hydroxyapatite powder were suspended in 4 mL 5% sterile Bovine Serum Albumin (BSA) solution, sonicated for 1 h at 40kHz and diluted in culture medium at final concentration of 62.5 µg/mL. The nHap suspension was characterized by dynamic light scattering that revealed a nanoparticles hydrodynamic diameter of 98 ± 30 nm as previously described.[13] nHap structure and morphology was evaluated by XRD and TEM analysis, respectively, as shown in **Figure 1 SI**. 10 µL of the suspension was deposited on a formvar coated copper grid (Electron Microscopy Sciences), and air-dried overnight. Images of the sample were acquired by Zeiss EM 10 transmission electron microscope operating at 80 kV. The XRD pattern, measured using a X ray wavelength of 1.5405 Å, shows the Hydroxyapatite, $Ca_5(PO_4)3(OH)$, crystal structure with space group P63/m and cell parameters a = b = 9.418 Å, c = 6.884 Å, α = β = 90° and γ = 120°.

2.3. *Cell Culture Conditions*

A density of 5 x 10^5 cells/cm^2 was used for experiments; cells were seeded on Thermanox (Nunc) supports for X-ray diffraction analysis, glass coverslips for fluorescence analysis while tissue culture plates for gene expression. After seeding, cells were kept in proliferative medium for 72 h and then osteoblast differentiation was induced using osteogenic medium: α-MEM (Invitrogen, Paisley, PENN) supplemented with 10% fetal bovine serum, 50 µg/mL penicillin-streptomycin, 2% L-glutamine, 2% Sodium Pyruvate, 10^{-7} M dexamethasone, 50 µg/mL ascorbic acid, and 5 mM b-glycero-phosphate.[14] Cells kept for 72 h after seeding in proliferative medium were used as time zero samples. Cells were cultured for 8 and 28 days in absence (Ctrl-8 and Ctrl-28) and presence of nHap (nHap-8 and nHap-28), previously suspended in culture medium at 62.5 µg/mL concentration.

2.4. Gene expression

To compare gene expression of cells during differentiation, same amount of cells cultured for 8 and 28 days in presence and absence of nHap, were harvested and total

View Article Online
DOI: 10.1039/C7NR05013E

RNA was extracted with the RNeasy Plus Mini Kit (Qiagen, Hilden, Germany). Reverse transcription was performed on 500 ng of total RNA by High Capacity cDNA Reverse Transcription Kit (Thermo Fischer Scientific, Carlsbad, US). Quantitative Real-time PCR (qrtPCR) was performed in a 96-well optical reaction plate in a 7500 Fast Real-Time PCR System (Applied Biosystems) using single tube Taqman real-time PCR assays (Thermo Fischer Scientific, Carlsbad, US), or in a MiniOpticon Real-Time PCR System (BioRad Laboratories) using SYBER Green qPCR (Stratagene, La Jolla, CA) (Table I SI). For SYBR-Green qPCR, reactions were performed in 20 µL with 2 µL of cDNA, 10 µL Brilliant SYBER Green qPCR Master Mix (Stratagene, La Jolla, CA), 0.4 µL of each primer, and 7.2 µL H2O. PCR conditions were as follows: 3 min at 95°C, 40 cycles of 5 sec at 95°C, and 23 sec at 60°C. Each sample was analyzed in triplicate, and the reaction mixture, without cDNA, was used as a negative control in each run.

2.5. Alkaline Phosphatase (ALP) activity and Von Kossa dual staining

After 8 and 28 days, cells were fixed with 4% PFA and washed with PBS. For ALP enzyme staining, samples were incubated for 30 min at room temperature with 0.01% Naphthol AS-MX Phosphate (Sigma) and 0.06% Fast Blue BB Salt. After extensive washing, cells were incubated for 5 minutes with 5% silver nitrate solution under the daylight and washed with distilled water 3 times. Samples were observed under the inverted microscope Olympus CX41 and pictures acquired at a 20X and 40X magnification with camera Olympus SP500UZ.

2.6 Calcium–cresolphthalein complexone assay

In order to quantify the mineral content of nHap treated and untreated samples, a Calcium Fast kit (Mercury SPA, Naples, Italy) was used according to the manufacturer's instructions. The colorimetric end point assay measures the amount of purple-coloured calcium–cresolphthalein complexone complex formed when cresolphthalein complexone binds to free calcium in an alkaline solution.[15] Briefly, 1 mL of 1N HCl was added to each sample at the end of the indicated times and incubated for 24 h at 4°C to release calcium into solution. The sample supernatant was diluted 1:10 with the Assay Working Solution previously prepared by mixing equal parts of calcium-binding reagent and calcium buffer reagent provided by the kit. Ca^{2+} standards in concentrations ranging from 0 to 10 mg/mL were prepared from dilutions of a 100 mg/mL stock solution of Ca^{2+}. The absorbance reading was performed at 595 nm with a microplate reader (BioRad Laboratories) using 100 µL of standard or sample placed into individual wells of a 96-

View Article Online
DOI: 10.1039/C7NR05013E

well plate. Samples were run in triplicate and compared against the standard solution calibration curve. Calcium quantification was performed at day 8, 14, 21 and 28 on untreated and nHap treated samples. Since the results at day 8 and 28 better represented the earlier and later process of mineralization of hBM-MScs with nHap, these time points were shown (**Fig. 2 SI)**.

2.7 Confocal Laser Scanning Microscopy (CLSM)

At the end of culture time, untreated (Ctrl-8 and Ctrl-28) and nHap treated (nHap-8 and nHap-28) samples were fixed with 4% PFA for 30 min at +4°C and washed with PBS three times. For immunological studies[16], PFA fixed cells were blocked by incubation with PAT (PBS containing 1% [w/v] bovine serum albumin and 0.02% [v/v] Tween 20) for 2 h at room temperature. Anti–type-I collagen, anti-osteocalcin and anti-decorin rabbit polyclonal antisera were kindly provided by Dr. Larry W. Fisher (http://csdb.nidcr.nih.gov/csdb/antisera.htm, National Institutes of Health, Bethesda, MD) and used as the primary antibodies diluted to 1:500 in PAT. The incubation with the primary antibodies was performed overnight at +4°C, whereas the negative controls were incubated with PAT alone. The samples and the negative controls were washed and incubated with Alexa-Fluor-488 goat anti-rabbit IgG (HþL; Invitrogen) at a dilution of 1:500 in PAT for 1 h at room temperature. At the end of the incubation, the samples were washed in PBS and counterstained with a Hoechst solution (2 μg/mL) to target the cellular nuclei. The images were acquired by the Fluorescence microscope (Leica Microsystems, Bensheim, Germany) equipped with a digital image capture system at 40X magnification.

2.8 Extraction of bone ECM proteins and enzyme-linked immunosorbent assay (ELISA)

At the end of the culture period (28 days), in order to evaluate the amount of deposited ECM, both types of samples were washed extensively with PBS to remove culture medium, and then incubated with sterile lysis buffer made of 20mM Tris-HCl, 4M GuHCl, 10mMEDTA, 0.066% [w/v] sodium dodecyl sulfate [SDS], pH 8.0. After that, the total protein concentration of samples was evaluated with the BCA Protein Assay Kit (Pierce Biotechnology, Inc., Rockford, IL).

Calibration curves to measure Col-I and Col-III, DCN, OPN, OCN, ONT, fibronectin (FN) and ALP were performed. Microtiter wells were coated with increasing concentrations of each purified protein, from 10 ng to 2 mg, in coating buffer (50mM Na_2CO_3, pH 9.5)

View Article Online
DOI: 10.1039/C7NR05013E

overnight at 4°C. Control wells were coated with BSA as a negative control. To measure the ECM amount of each protein by ELISA, microtiter wells were coated, overnight at 4°C, with 100 µL of the previously extracted ECM (20 µg/mL in coating buffer).[17] After three washes with PBS containing 0.1% (v/v) Tween 20, the wells were blocked by incubating with 200 µL of PBS containing 2% (w/v) BSA for 2 h at 22°C. The wells were subsequently incubated for 1.5 h at 22°C with 100 µL of the anti-type-I and -III collagens, anti-decorin, anti-osteopontin, anti-osteocalcin, anti-osteonectin and anti-ALP rabbit polyclonal antisera (1:500 dilution in 1% BSA), kindly provided by L. Fisher. The same dilution was used for the anti-FN rabbit polyclonal IgG. After washing, the wells were incubated for 1 h at 22°C with 100µL of horseradish peroxidase (HRP)-conjugated goat anti-rabbit IgG (1:500 dilution in 1% BSA). The wells were finally incubated with 100 µL of the development solution (phosphate-citrate buffer with ophenylenediamine dihydrochloride substrate). The color reaction was stopped with 100 µL of 0.5 M H_2SO_4, and the absorbance values were measured at 490nm with a microplate reader (BioRad Laboratories).

2.9 Statistical Analysis

Experiments for quantitative evaluation of calcium and bone matrix proteins deposition and gene expression were repeated three times. Results are expressed as the mean ± standard deviation. In order to compare the results between nHap and Ctrl samples, the one-way analysis of variance (ANOVA) with *post hoc* Bonferroni test was applied, with a significance level of 0.05.

2.10 Synchrotron micro X-ray diffraction measurements and data analysis

After 8 and 28 days of differentiation control and treated samples were fixed with 4% (w/v) paraformaldehyde (PFA) solution in 0.1 M phosphate buffer (pH 7.4) (PBS) for 30 m at +4°C, washed with PBS and bi-distilled water and dry overnight.

The SµXRD measurements were carried out the ID13 beamline at the European Synchrotron Synchrotron Radiation Facility (ESRF) in Grenoble, France. A schematic of the experimental apparatus is shown in **Figure 3 SI**. The scanning micro-diffraction setup, equipped with a Si(111) channel cut monochromator and Compound Refractive Lenses as focusing system, supplied a beam size of 2x2 µm with a wavelength of 13.9 keV. The sample was mounted at a distance from the detector of 149.25 mm. The beam center, detector tilt and sample-to-detector distance were calibrated using the Al_2O_3 standard. 2D X-ray diffraction frames have been collected in transmission by using a

View Article Online
DOI: 10.1039/C7NR05013E

fast Eiger 4M detector (Dectris), allowing us to acquire each diffraction image with an exposure time of 50 ms. The samples were scanned by a step motor stage with 0.1 micron repeatability using a step size of 2 μm in both vertical, z, and horizontal, y, direction. In each point reached by the y-z translator we collected a 2D diffraction frame diffraction.

We selected several Regions Of Interest (ROI) from three different cell cultures at 8 and 28 days, with (nHAP-8, nHAP-28) and without (Ctrl-8, Ctrl-28) nHAP addition, covering a total surface measurements of 0.2 mm^2 for each sample type: Ctrl-8, Ctrl-28, nHap-8 and nHap-28.

We measured also several ROIs in time zero samples, with cell cultures at 2 days, in order to assess and subtract the background from the data normalized for the incident flux. The 2D diffraction patterns have been radially integrated and background subtracted to provide 1D profiles of intensity, I(q), vs. transfer moment, $q=4\pi\sin(\theta)/\lambda$, (see **Figure 1a)**. We have integrated 2D data using a Δq of 0.027 nm^{-1}, allowing us to cover a quite large q-range from 0.25 nm^{-1} to 45 nm^{-1}. **Figure 4 SI** in the Supplementary Information shows the thermanox background SAXS signal and the SAXS patterns normalized and subtracted by the background in four different points of a nHAP-28 sample. We get clear orientation in the thermanox SAXS signal (see Fig. 4 SI a, Fig. 4 SI c). Anyway, the thermanox SAXS signal subtraction, after normalization, gives weak signal, near to zero, in the zones without mineralization (see pattern 1 in Fig. 4 SI d, Fig. 4 SI e, Fig. 4 SI f).

The mineralization degree, related to the cells differentiation rate, is measured by the SAXS invariant

$$Q = \int_{q(SAXS_1)}^{q(SAXS_2)} q^2[I(q) - I_{BKG}(q)]dq \qquad (1)$$

defined in the region from $q(SAXS_1)$=0.25 nm^{-1} to $q(SAXS_2)$=5.5 nm^{-1}. The achieved q range of [0.25-45] nm^{-1} allowed us to measure simultaneously both the SAXS and the WAXS signal for investigating structure from nano to atomic scale. The crystallinity of the deposited mineral nanostructure was verified by measuring the more intense reflections of hydroxyapatite hexagonal P6/m structure with cell parameters a=9.4162 Å and c=6.8791 Å. Broad and overlapping peaks of the more intense reflections 211, 112, 300 of Hap are shown in **Figure 1b**, indicating the crystalline nature of the measured nanostructure. The WAXS signals are constituted by 2D spots. The fact that we got spots and not rings tell us that the hydroxyapatite nanocrystals form micrograins with strong crystallographic textures, which can be observed only when micrograins are

View Article Online
DOI: 10.1039/C7NR05013E

properly oriented. Anyway, the cross correlations between the crystallographic textures, the oriented polymer fibers of the thermanox support (see Fig. 4 SI), and the extracellular collagenous matrix will be discussed elsewhere and are not included in the issue of this paper.

2.11 Synchrotron micro X-ray Fluorescence measurements and data analysis

The X-ray Fluorescence signals were collected simultaneously to the X-ray diffraction by a Vortex silicon drift detector with energy resolution of 136 eV (FWHM at Mn K_α) and a XIA electronic system providing 4096 channels with bin width of 50 eV for each channel (see the scheme of the experimental set up in **Figure 3 SI)**. The peaks corresponding to the Calcium electronic K_α and K_β levels are shown in **Figure 1c**. The area of the peaks can be associated to the Calcium content, point by point.

2.12 Spatial Statistics

The Probability Density Function, PDF, of the deposited hydroxyapatite content in the different samples, has been used to describe the nucleation and growth of hydroxyapatite nanocrystals in the different ROIs. On the same ROIs the possible spatial correlations has been performed by calculating the spatial correlation function G(r) describing the probability of finding a domain with hydroxyapatite deposited at a particular distance r from another domain with hydroxyapatite deposited. To obtain G(r), we have first calculated the correlations of any pairs of spots in the 2D image separated by the vector $\vec{r} = \vec{R}_i - \vec{R}_j$ in the x-y plane, following the expression:

$$G(\vec{r}) = \frac{1}{N(\vec{r})} \sum_{i,j} \delta_{r,\ \overrightarrow{R(i)}-\overrightarrow{R(j)}} \frac{(I_i - \langle I \rangle_1)(I_j - \langle I \rangle_2)}{\sigma_1 \sigma_2} \qquad (1)$$

where $N(\vec{r}) = \sum_{i,j} \delta_{r,\ \overrightarrow{R(i)}-\overrightarrow{R(j)}}$ indicates the number of points at distance $\vec{r} = \vec{R}_i - \vec{R}_j$.

The average intensities are calculated according to the expressions

$$\langle I \rangle_1 = \frac{1}{N(\vec{r})} \sum_{i,j} \delta_{r,\ \overrightarrow{R(i)}-\overrightarrow{R(j)}} I_i \ = \ \langle I \rangle_2 = \frac{1}{N(\vec{r})} \sum_{i,j} \delta_{r,\ \overrightarrow{R(i)}-\overrightarrow{R(j)}} I_j \qquad (2)$$

and the standard deviation are calculated according to:

$$\sigma_1^2 = \left(\frac{1}{N(\vec{r})} \sum_{i,j} \delta_{r,\ \overrightarrow{R(i)}-\overrightarrow{r(j)}} I_i^2 \right) - \langle I \rangle_1^2; \quad \sigma_2^2 = \left(\frac{1}{N(\vec{r})} \sum_{i,j} \delta_{r,\ \overrightarrow{R(i)}-\overrightarrow{R(j)}} I_j^2 \right) - \langle I \rangle_2^2 . \qquad (3)$$

Finally, we take $G(r) = \langle G(\vec{r}) \rangle$ where the average is over all the allowed directions in the grid describing the 2D image.

View Article Online
DOI: 10.1039/C7NR05013E

We compared the spatial correlations G(r) of ROIs spatial patterns with the G(r) of Complete Spatial Randomness (CSR) given by the G(r) calculated on shuffled spatial patterns.

Afterwards, the deposited hydroxyapatite, assembling to form grains at micrometric scale, have been studied by calculating the position, area and mean Q value of each grain. We individuated and located grains selecting the pixel intensity values higher than the threshold given by the maximum Q value obtained for the background. In this way, we defined the population of the deposited nanocrystals, N_{Hap}, in each grain by <Q>A where <Q> is the mean value of the Q invariant on the grain area and A is the area of the grain.

3. Results

3.1. Gene expression and protein composition during ECM extracellular matrix formation and mineralization

In vitro differentiation of hBM-MSCs to osteoblast occurs in the presence of dexametasone, beta-glycerol phosphate and ascorbic acid within 28 days. Differentiated osteoblasts express ALP and form three-dimensional ECM that becomes mineralized. By day 8, all differentiating cells show positive ALP activity, while mineralization starts around day 14 with deposition of hydroxyapatite nanocrystals.[18,19] Therefore, we have chosen to analyze hBM-MSCs' differentiation at both day 8 and 28 in order to compare cells actively producing bone matrix (day 28) with early differentiating cells (day 8), and to evaluate the effects of added nHap on bone matrix deposition.

At molecular level, differential expression of bone-related genes has been assessed by quantitative real time Polymerase Chain Reaction (PCR). The results, shown in **Figure 2**, reveal an enhancer effect of nHap on the accumulation levels of the bio-marker genes *ALP*, integrin binding sialoprotein (*IBSP)*, *OCN* and *DCN* reaching the highest value after 28 days of differentiation.

At the same time, remodeling of gene expression parallels the increase of the corresponding proteins and also other specific bone ECM proteins, including type-III

View Article Online
DOI: 10.1039/C7NR05013E

collagen (Col-III) that are significantly higher in nHap-28 compared to Ctrl-28 samples as reported in **Table I**. To visualize bone matrix protein distribution, Col-I, OCN and DCN were immunostained and observed by Confocal Laser Scanning Microscopy (CLSM). A noteworthy difference is present between 8 days and 28 days samples (Ctrl vs nHap). In particular, at day 8, Col-I appears localized at cellular level in both Ctrl and nHap samples, namely Ctrl-8 and nHap-8, whereas at day 28, a well-formed ECM, with fibrillary character is clearly visible in both Ctrl and nHap samples (Ctrl-28 and nHap-28, **Figure 3**). The increasing of other bone ECM proteins such as OCN and DCN can be visualized in CLSM images of **Figure 5 SI**, by the less intense green fluorescence present in Ctrl-8 and nHap-8 samples, in comparison with the Ctrl-28 and nHap-28.

The relative amount of calcium (Ca) deposition in the matrix has been quantified by calcium–cresolphthalein complexone assay; furthermore, ALP activity and Ca (Von Kossa) were evaluated by dual staining of both Ctrl and nHap treated samples (**Figure 2 SI**). In **Figure 2 SI a,** we show that after 8 days no mineralization is visible on Ctrl and nHap samples, while an intense blue staining indicating ALP activity, strictly correlated to hBM-MSCs differentiation toward osteoblasts, is present. After 28 days, both Ctrl and nHap present an intense dark staining, demonstrating strong mineral deposition. From a quantitative point of view, nHap-28 samples display a significant higher Ca deposition compared to Ctrl-28 (**Figure 2 SI b**).

3.2. Spatiotemporal evolution of hBM-MSCs to osteoblast differentiation during ECM mineralization

The mineralization process has been studied by monitoring the differentiation process of hBM-MSCs at higher spatial resolution on micrometric and nanometric scale. At this aim, we have measured the spatiotemporal evolution of HAP nanocrystals deposited in the ECM, in the Ctrl-8, nHap-8, Ctrl-28 and nHap-28 samples by simultaneous SμXRD and SμXRF (see Methods and Materials). Typical Small/Wide angle X-ray scattering (SAXS, WAXS) and X ray Fluorescence (XRF) profiles measured at different samples spots are shown in **Figure 4a, 4b** and **4c** respectively. The HAP nanocrystal content has been evaluated through both the Q invariant (that measures the mineralization degree related to the cells differentiation rate) calculated by eq. 1 (see Materials and Methods), and the Ca content quantified with the area of Ca K_α and K_β peaks in the XRF profiles.

View Article Online
DOI: 10.1039/C7NR05013E

Typical maps of Q calculated in 200x200 μm^2 region of interest (ROIs) for the control and nHap treated samples, are shown in **Figure 4a**. To be ensured about the nature of the collected SAXS signals, we have compared the Q maps with the Ca maps, measured simultaneously by SμXRF, obtaining fully correlations for all ROIs, indicating that the collected SAXS signals from nanostructures was actually due to the hydroxyapatite nanocrystals deposited by differentiated cells (see **Figure 6 SI)**. Q and Ca maps evaluation clearly indicates that the deposited hydroxyapatite nanocrystals became increasingly extensive in nHap-8 and nHap-28 treated samples, compared to controls, Ctrl-8 and Ctrl-28, in agreement with von Kossa measurements.

We have characterized the cell differentiation dynamics through the evolution of the spatial distribution of the deposited nanocrystals, calculating *i*) the Probability Density Function (PDF) of deposited nanocrystal content, *ii*) the spatial correlations within the spatial patterns and *iii*) the organization of deposited nanocrystals in micro grains.

The PDF evolution of the amount of deposited nanocrystals is shown in **Figure 4b**. The PDF calculated in the Ctrl samples has been fitted using the exponential function $Ce^{-Q/\tau}$ whit constant C and $\tau = 0.07$ representing the characteristic decay value for the Q invariant. The exponential distribution indicates a random memoryless process, in which nanocrystal subpopulations increase independently by the others, both in time and in space. As the bio-mineralization degree increases, we can observe larger aggregates and higher number of deposited grains. This different dynamic regime is described by the PDF evolution that changes its shape from an exponential to a power-law given by $PDF(Q) = Q^{-\alpha}$, where α is the critical exponent. The PDFs have been fitted to derive maximum likelihood estimates of the lower bound and exponent of the distribution.[20] We observe a clear elongation and fattening of the right tail distribution, with the reduction of the power law exponent from -3.4 in the nHap-8 samples to -2 in the nHap-28 samples. Also the Ca results are spatially distributed with a power law behavior with exponent -2.0±0.2, as shown in **Figure 4b**.

The spatial correlations within the spatial pattern, when complete cell differentiation is approaching, have been quantified by the spatial correlation function G(r) in the Ctrl-8, Ctrl-28, nHap-8 and nHap-28 samples (see **Figure 4c**). All the G(r) curves show a fast exponential decay on the “complete spatial randomness” (CSR) regime indicated by the

View Article Online
DOI: 10.1039/C7NR05013E

green zone, except for the nHap-28 samples. In particular, in the Ctrl ROIs, the G(r) decays at distances $r < 3$ μm, while in the nHap-8 ROIs the correlations show a light increasing, being $r > 4$ μm consistent with the occurrence of the first aggregation nuclei. On the other hand, we find persistent correlations decaying on the CSR zone at distances of about $r \cong 20$ μm in the nHap-28 samples. We can associate this exponential length distribution, from 2 to 20 mm, to the size of micrometric grains formed by assembled Hap nanocrystals deposited by differentiated osteoblasts. Beyond the exponential decay, spatial correlations peaks at larger r are absent in both the Ctrl and the nHap-8 samples, but appear as a Gaussian centered at $R_c = 43$ μm in the nHap-28 samples. This suggests that hydroxyapatite micrograins have a spatial organization and are distributed around the inter-grains distance of $R_c \pm \Delta R_c/2$ where $\Delta R_c = 4$ μm is the Full Width at Half Maximum (FWHM) of the Gaussian peak. This organization could be due to the osteoblasts cells packing where the osteoblast size is consistent with R_c.[21]

In order to deepen the spatial organization of deposited hydroxyapatite nanocrystals in micro grains, we have characterized quantitatively both the HAP nanocrystal *population* and the size for each grain. In **Figure 5a** we show the scatter plot of <*Q*> vs the area of all grains, measured in all ROIs. We observe the increased points density in the nHap-28 grains, in the shadowed area extending towards higher grain area values. The grain density and the nanocrystal populations are represented in **Figure 5b**. We can clearly observe how the nHap nanoparticle addition promotes the hBM-MSC differentiation in osteoblast with an increase of hydroxyapatite deposition. Indeed, both the grains density and the hydroxyapatite population are found to be higher in the nHap-28 sample and decreases monotonically in the nHap-8, Ctrl-28 and Ctrl-8 samples. Anyway, beyond the clear trend of the differentiation degree, we can find grains more mineralized in the sample at 8 days and grain less mineralized at 28 days both in the Ctrl and in the nHap samples. This non-homogeneous behavior arises from an intrinsic heterogeneity of the fate rate of cell subpopulations.[22,23]

4. Discussion

hBM-MSCs are multipotent stem cells which can be differentiated into multiple lineages according to the surrounding environments.[24-27] In this framework, the control and

View Article Online
DOI: 10.1039/C7NR05013E

manipulation of the spatiotemporal differentiation cover a great relevance in different reason spanning from basic science[28] to applicative biomedicine such as tissue engineering and regenerative medicine.[29-31] Bone tissue regeneration has pressing scientific and social impact, since bone grafts are the most common transplants after the blood transfusions. Thus, the understanding of bone tissue regeneration assumes a paramount importance both in basic material research and in biomedicine.

In this work we have studied the hBM-MSCs differentiation process assessing the possibility to control the space and fate rate by exogenously applied nHap. The addition of nHap in the cell culture increased the synthesis and deposition of ALP, OCN, DCN and Col-III, promoting a greater deposition of these proteins, which are strictly related to the ECM mineralization.[16] To confirm the close relationship between bone matrix proteins and mineral deposits, OCN and DCN resulted more concentrated in specific areas of the samples, likely in correspondence to the hydroxyapatite deposits as already reported by other authors.[32] Von Kossa staining highlighted macroscopically the increased amount of mineral deposits by the presence of nHap.

The nucleation, growth and reorganization of mineralization centers, has been visualized at higher spatial resolution, at micrometric and nanometric scale, measuring the deposition of nanocrystals by simultaneous Scanning micro X-Ray Diffraction and Scanning micro X-Ray Fluorescence. The unique features of Synchrotron radiation such as the high brilliance, allow to detect weak signals from small amount of sample onto small (sub)micrometric spot size, as occurs in our case, where samples to probe are nanocrystals deposited by a cell monolayer. Furthermore, the low divergence allows measuring a large range in the reciprocal k-space, collecting simultaneously both Small Angle X-ray Scattering (SAXS) and Wide Angle X-ray Scattering (WAXS) signals giving structural information at nano and atomic scale, respectively. In addition, thanks to the X-ray advanced focusing optics, it is possible to focus the X-ray photons on micrometric spot and scan the sample to map structural features in real space, at microscale. Thus, probing both the k-space and real space, SμXRD allow us to visualize structural features from atomic and nanometric scale up to microscale. The high synchrotron radiation flux and the feasibility of the ID 13 beamline allow also recording the weak Ca signal from the cell monolayers, using Scanning micro X-ray Fluorescence (XRF). Taking advantage of all these features, we have been able to monitor the mineralization degree, correlated to the cell differentiation process according to its spatial and

View Article Online
DOI: 10.1039/C7NR05013E

temporal evolution. The nanocrystal nucleation and growth in the Ctrl samples showed an exponential probability distribution function, typical of random memoryless homogeneous process. As the differentiation process was completing, the probability distribution of the forming hydroxyapatite nanocrystals changed shape passing from an exponential to a power law typical of complex and self-organized process. During this differentiation process, the deposited nanocrystals assembled in micrograins showing a tendency to organize in clusters.

The complexity of this process requires other deeper studies to clarify the combination of local molecular interactions leading to spatiotemporal self-organised patterns of differentiated stem cells to osteoblasts. In this context, a widely accepted mechanism proposed for bone mineralization e.g. hydroxyapatite deposits in ECM, states that the extracellular matrix vesicles (MVs) are the site of initial or primary nucleation. Biomineralization is essentially a biphasic phenomenon: *phase 1* is concerned with the formation of the first crystals of mineral within MVs; *phase 2* begins with crystal penetration of the MV membrane, exposing preformed mineral to the extracellular fluid.[33] The rate of the mineral crystal proliferation from this point was reported to be controlled by extracellular conditions such as the levels of ionic Ca^{+2} and PO_4^{3-}, the pH and the presence of organic molecules (proteoglycans and several non-collagenous calcium-binding proteins of bone including OCN, phosphoproteins, ONT, and alpha-2-HS-glycoproteins).[34] In particular, it may be possible that the addition of nHAP to the cell cultures might influence both phase 1 and phase 2 of ECM mineralization process. The continuous treatment with nHap during the cell culture, when mineralization process has already started, may influence also the mineralization centers leading to a different organization of mineral deposits in the ECM that we observed with X-rays. However, future in vitro experiments may be performed using differentially substituted nHap to validate this model.

Conclusions

In this work, we show for the first time the effect promoted by the presence of exogenously added nHAP on hBM-MSCs' mineralization process measuring the newly deposited hydroxyapatite nanocrystals at 2 times points (e.g. 8 and 28 days) by simultaneous Scanning micro X-Ray Diffraction and Scanning micro X-Ray

View Article Online
DOI: 10.1039/C7NR05013E

Fluorescence. Biologically speaking, both gene expression profiling of bone specific markers and protein deposition were actively promoted by the addition of nHap during hBM-MSCs' differentiation process. In this context, we have been able to characterize the cell differentiation dynamics through the evolution of the spatial distribution of the deposited nanocrystals. These results show the complex nature of differentiation dynamics, associated with i) the power law behavior of deposited hydroxyapatite nanocrystal growth, ii) the development of longer spatial correlations in the nHap-28 samples and iii) the non-homogeneous fate rate of cell subpopulations.

This study expected to provide an evaluable contribution to a deeper understanding of the stem cell differentiation dynamics, opening new possibilities to control the progression of the degenerative diseases through the tissue engineering and regenerative medicine.

Acknowledgments

Cell biology, biochemistry and molecular biology studies were supported by grant from the Italian Space Agency Project DC-MIC-2012-024, contract N. 2013-060-I.O to G.R., A.M.R. and L.V. We thanks the ID13 staff for the technical help and assistance.

Author Contributions

G.R., A.M.R. and L.V. conceived the project and designed all the experiments. G.C., A.C. and M.F. contributed to the planning of the experiments. The samples were grown and characterized by F.C., G.P., B.P. and PAC. Scanning micro X-Ray Diffraction and Fluorescence measurements have been carried out at ID13-ESRF by G.C., F.C., G.P., M.F. and B.W. X Ray Diffraction and Fluorescence data analysis has been done by G.C. All authors discussed the results and worked on the interpretation of the data. The manuscript has been written by G.C., A.M.R., L.V. and G.R collecting feedback from all the authors.

View Article Online
DOI: 10.1039/C7NR05013E

Table I Extracellular matrix proteins secreted and deposited in Ctrl-28 and nHap-28 samples of hBM-MSCs expressed in pg/cell.

	Matrix protein deposition after 28 days of cell culture [expressed as pg/cells]		
Protein	**Ctrl-28**	**nHap-28**	**Ratio nHap/Ctrl**
Alkaline Phosphatase	25.40 ± 1.3	30.91 ± 1.5 **	1.2
Osteocalcein	3.41 ± 0.2	3.93 ± 0.4 *	1.2
Decorin	112.1 ± 13.1	129.5 ± 5.6 *	1.2
Osteopontin	3.80 ± 2.0	3.88 ± 0.2	1.0
Osteonectin	3.92 ± 0.0	3.82 ± 0.5	1
Type-I Collagen	58.4 ± 2.6	45.9 ± 0.7	0.8
Type-III Collagen	150.9 ± 10.0	170.4 ± 8.2 *	1.1

Ratio between nHap-28 and Ctrl-28 is reported in the third column. Statistical analysis was performed against Ctrl-28 (*p<0,05, **p<0,01; n=3).

View Article Online
DOI: 10.1039/C7NR05013E

Figures and figure legends

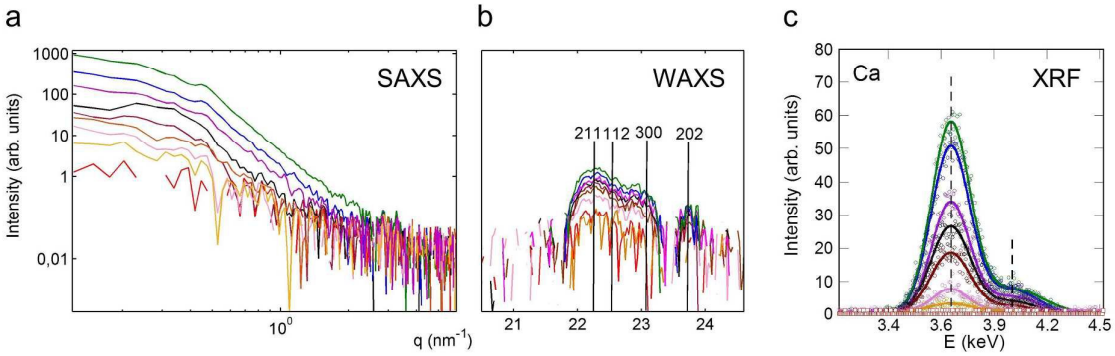

Figure 1: SAXS, WAXS and XRF profiles measured at different spots.

(**a**) Typical Small Angle X ray scattering profiles, in Log-log scale, measured on different 2x2 μm^2 spots with different content of hydroxyapatite nanoparticles. (**b**) Wide Angle X Ray Diffraction profile in a semi-logarithmic scale. The broad weak hydroxyapatite peaks indicated the crystallinity at nanoscale. (**c**) X ray Fluorescence corresponding to the Calcium K_α and K_β electronic levels, measured on the 2x2 μm^2 spots of A and B.

View Article Online
DOI: 10.1039/C7NR05013E

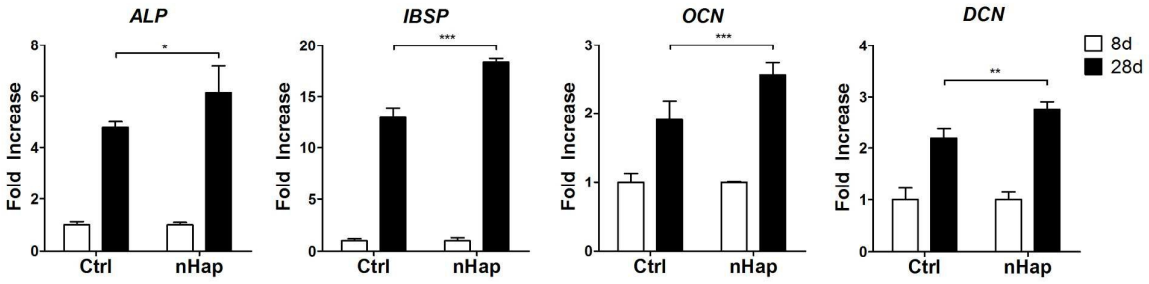

Figure 2: Differential gene expression profiling of bone specific markers during differentiation. Expression levels were determined by qrtPCR in Ctrl-8, Ctrl-28, nHap-8 and nHap-28 samples of hBM-MSCs. The graph shows the fold induction of gene expression expressed in arbitrary units. Bars indicate mean and SEM of three different experiments. Statistical analysis was performed against controls (Ctrl-8 and Ctrl-28) (*p<0,05, **p<0,01, ***p<0,001; n=3)

View Article Online
DOI: 10.1039/C7NR05013E

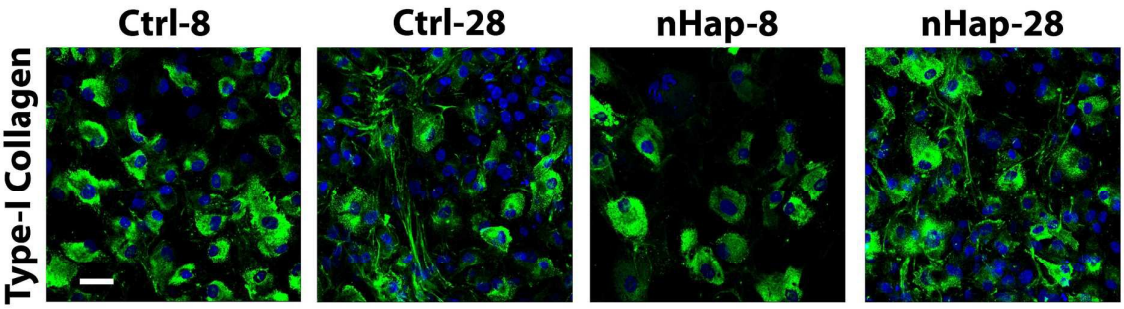

Figure 3: **Deposition of type-I collagen in hBM-MSCs during differentiation.**

CLSM images of hBM-MSCs immunostaining of collagen I deposited in Ctrl-8, Ctrl-28, nHap-8 and nHap-28. hBMSCs were seeded and incubated without/with nHap suspensions for 8 and 28 days, respectively. At the end of each incubation time, cells were fixed and immunostained against type-I collagen as indicated in Materials and Methods section. Nuclei were counterstained with Hoechst 33342 (blue) and the extracellular deposits of type-I collagen was probed with a fluorescent secondary antibody (green). The white bar corresponds to 50 μm.

View Article Online
DOI: 10.1039/C7NR05013E

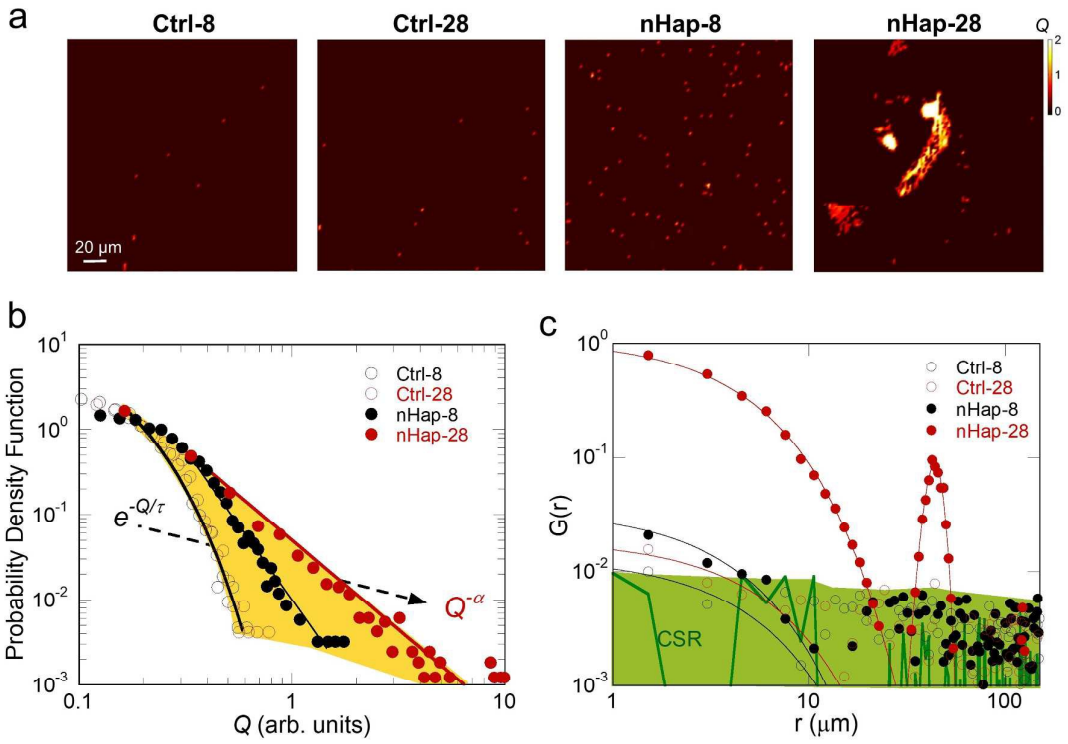

Figure 4: Emergence of complexity during by human bone marrow mesenchymal stem cells differentiating toward osteoblasts.

(**a**) Maps of the Q invariant measured on the Ctrl-8, Ctrl-28, nHap-8 and nHap-28 samples. (**b**) Probability Density Function calculated for the Q maps of samples. The shadowed area crossed by the arrow indicates the transition from random hydroxyapatite nanocrystals formation (in ctrl samples) described by an exponential probability density function to a complex spatially correlated growth, described by a power law regime, with critical exponent α=-2. (**c**) Spatial correlation function, G(r), of deposited hydroxyapatite nanocrystals indicating how spatial persistent correlations in cell differentiation occur going from Ctrl-8 to nHap samples, crossing the yellow shadowed area. The G(r) calculated for a Complete Spatial Randomness is also shown, indicated by the green thick line in the green shadowed area. The G(r) curves show a fast exponential decay on the "complete spatial randomness" (CSR) regime indicated by the green zone, except for the nHap-28 samples where we find a slower decay and a pronounced peak, associated with the inter clusters length of r ≅ 43 ± 4 μm. The continuous lines represent the exponential fitting curves, with the addition of a Gaussian line shape in the nHap-28 sample.

View Article Online
DOI: 10.1039/C7NR05013E

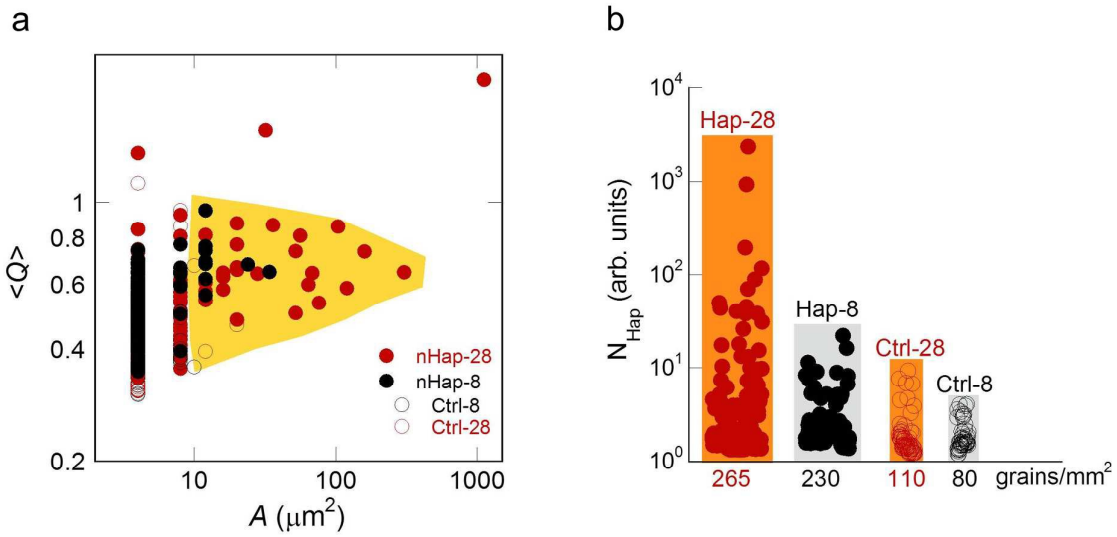

Figure 5: Micro grain analysis of deposited nanocrystals.

(**a**) Mean Q value, <*Q*>, vs area of each grain measured in a total area of 0.2 mm^2 on the Ctrl-8, Ctrl-28, nHap-8 and nHap-28 samples. (**b**) Particle total population, nHap, in each grain, *i*, given by *A(i)**<*Q(i)*> as a function of the grain density for the different samples.

View Article Online
DOI: 10.1039/C7NR05013E

REFERENCES

1. P. Ducy, R. Zhang, V. Geoffroy, A. L. Ridall and G. Karsenty, Cell, 1997, 89, 747-754.
2. M. Capulli, R. Paone and N. Rucci, Arch Biochem Biophys, 2014, 561, 3-12.
3. D. T. Denhardt and X. Guo, FASEB J, 1993, 7, 1475-1482.
4. T. Matsuguchi, N. Chiba, K. Bandow, K. Kakimoto, A. Masuda and T. Ohnishi, J Bone Miner Res, 2009, 24, 398-410.
5. G. Campi, M. Fratini, I. Bukreeva, G. Ciasca, M. Burghammer, F. Brun, G. Tromba, M. Mastrogiacomo and A. Cedola, Acta Biomater, 2015, 23, 309-316.
6. G. Campi, A. Ricci, A. Guagliardi, C. Giannini, S. Lagomarsino, R. Cancedda, M. Mastrogiacomo and A. Cedola, Acta Biomater, 2012, 8, 3411-3418.
7. G. Campi, A. Bianconi, N. Poccia, G. Bianconi, L. Barba, G. Arrighetti, D. Innocenti, J. Karpinski, N. D. Zhigadlo, S. M. Kazakov, M. Burghammer, M. Zimmermann, M. Sprung and A. Ricci, Nature, 2015, 525, 359-362.
8. H. Li, H.-g. Xiao, J. Yuan and J. Ou, Composites Part B: Engineering, 2004, 35, 185-189.
9. G. Campi, G. Pezzotti, M. Fratini, A. Ricci, M. Burghammer, R. Cancedda, M. Mastrogiacomo, I. Bukreeva and A. Cedola, Applied Physics Letters, 2013, 103, 253703-253703.253704.
10. N. Poccia, G. Campi, A. Ricci, A. S. Caporale, E. Di Cola, T. A. Hawkins and A. Bianconi, Sci Rep, 2014, 4, 5430.
11. M. Fratini, G. Campi, I. Bukreeva, D. Pelliccia, M. Burghammer, G. Tromba, R. Cancedda, M. Mastrogiacomo and A. Cedola, Nuclear Instruments and Methods in Physics Research Section B: Beam Interactions with Materials and Atoms, 2015, 364, 93-97.
12. M. E. Bernardo, N. Zaffaroni, F. Novara, A. M. Cometa, M. A. Avanzini, A. Moretta, D. Montagna, R. Maccario, R. Villa, M. G. Daidone, O. Zuffardi and F. Locatelli, Cancer Research, 2007, 67, 9142-9149.
13. M. Frasnelli, F. Cristofaro, V. M. Sglavo, S. Dire, E. Callone, R. Ceccato, G. Bruni, A. I. Cornaglia and L. Visai, Materials science & engineering. C, Materials for biological applications, 2017, 71, 653-662.
14. M. E. Bernardo, M. A. Avanzini, C. Perotti, A. M. Cometa, A. Moretta, E. Lenta, C. Del Fante, F. Novara, A. de Silvestri, G. Amendola, O. Zuffardi, R. Maccario and F. Locatelli, J Cell Physiol, 2007, 211, 121-130.
15. S. A. Cohen, L. Sideman, Clin. Chem.,1979, 25, 1519–20.
16. M. Vercellino, G. Ceccarelli, F. Cristofaro, M. Balli, F. Bertoglio, G. Bruni, L. Benedetti, M. A. Avanzini, M. Imbriani and L. Visai, Nanomaterials, 2016, 6.
17. G. Ceccarelli, N. Bloise, M. Mantelli, G. Gastaldi, L. Fassina, M. G. De Angelis, D. Ferrari, M. Imbriani and L. Visai, BioResearch open access, 2013, 2, 283-294.
18. A. K. Majors, C. A. Boehm, H. Nitto, R. J. Midura and G. F. Muschler, J Orthop Res, 1997, 15, 546-557.
19. D. J. Rickard, M. Kassem, T. E. Hefferan, G. Sarkar, T. C. Spelsberg and B. L. Riggs, J Bone Miner Res, 1996, 11, 312-324.
20. A. Clauset, C. Shalizi and M. Newman, SIAM Review, 2009, 51, 661-703.

View Article Online
DOI: 10.1039/C7NR05013E

21. O.F. Zouani, L. Rami, Y. Lei, M. C. Durrieu, Biol Open, 2013, 2, 872-81.
22. P. Bogdan, B. M. Deasy, B. Gharaibeh, T. Roehrs and R. Marculescu, Sci Rep, 2014, 4, 4826.
23. Y. Han, T. Bai and W. Liu, Sci Rep, 2014, 4, 5815.
24. S. Namgung, K. Y. Baik, J. Park and S. Hong, ACS Nano, 2011, 5, 7383-7390.
25. M. F. Pittenger, A. M. Mackay, S. C. Beck, R. K. Jaiswal, R. Douglas, J. D. Mosca, M. A. Moorman, D. W. Simonetti, S. Craig and D. R. Marshak, Science, 1999, 284, 143-147.
26. D. E. Discher, D. J. Mooney and P. W. Zandstra, Science, 2009, 324, 1673-1677.
27. T. S. Stappenbeck and H. Miyoshi, Science, 2009, 324, 1666-1669.
28. L. a. S. J. Machado, A., Journal of Biomedical Science and Engineering, 2013, 6, 683-692.
29. C. Nombela-Arrieta, J. Ritz and L. E. Silberstein, Nat Rev Mol Cell Biol, 2011, 12, 126-131.
30. Y. Jiang, B. N. Jahagirdar, R. L. Reinhardt, R. E. Schwartz, C. D. Keene, X. R. Ortiz-Gonzalez, M. Reyes, T. Lenvik, T. Lund, M. Blackstad, J. Du, S. Aldrich, A. Lisberg, W. C. Low, D. A. Largaespada and C. M. Verfaillie, Nature, 2007, 447, 880–881.
31. V. F. Segers and R. T. Lee, Nature, 2008, 451, 937-942.
32. P. V. Hauschka and F. H. Wians, Jr., Anat Rec, 1989, 224, 180-188.
33. H. C. Anderson, Clin Orthop Relat Res, 1995, 266-280.
34. H. C. Anderson, Lab Invest, 1989, 60, 320-330.